scientific reports

Check for updates

OPEN

$A\beta_{42}$ induces stress granule formation via PACT/PKR pathway

Vijay Sankar Ramasamy[1]✉, Alan Benhur Pravin Nathan[2], Moon-Chang Choi[1], Sung-Hak Kim[3] & Takbum Ohn[1]✉

Stress granule (SG) formation has been linked to several neurodegenerative disorders, such as Alzheimer's disease (AD). Amyloid-β42 (Aβ42) is a key player in the pathogenesis of AD and is known to trigger various stress-related signaling pathways. However, the impact of Aβ on SG formation has not been fully understood. The primary aim of this study is to analyze the SG-inducing properties of Aβ42 and to uncover the molecular mechanisms underlying this process. Our results revealed that exposure to 20 µM Aβ42 led to a significant SG formation in neuroblastoma-derived (SH-SY5Y) and glioma-derived (U87) cell lines. Interestingly, we observed elevated levels of p-eIF2α, while overall protein translation levels remained unchanged. Monomeric and oligomeric forms of Aβ42 exhibited a 4–5 times stronger ability to induce SG formation compared to fibrillar forms. Additionally, treatment with familial mutants of Aβ42 (Dutch and Flemish) showed distinct effects on SG induction. Moreover, our findings using eIF2α kinases knockout (KO) cell lines demonstrated that Aβ-induced SG formation is primarily dependent on Protein Kinase R (PKR). Subsequent proximity ligation assay (PLA) analysis revealed a close proximity of PACT and PKR in Aβ-treated cells and in AD mouse hippocampus. Taken together, our study suggests that Aβ42 promotes SG formation through PKR kinase activation, which in turn requires PACT involvement.

Keywords Aβ42, Amyloid-β, Stress granule, PKR kinase, Alzheimer's, Stress signaling

Stress granules (SGs) are cytosolic assemblies that form in response to stress (e.g., heat, oxidative stress, hypoxia, viral infection and UV) and typically disperse after the stress is resolved[1–3]. SGs minimize stress-related damage and promote cell survival. SGs are composed of mRNA, RNA binding proteins (RBPs), 40S ribosomal subunits and translation initiation complexes[4]. The process of SG formation is initiated by core nucleating RBPs, including T-cell intracellular antigen 1 (TIA-1), tristetraprolin (TTP), and Ras-GTPase-activating protein SH3-domain-binding protein (G3BP)[5,6]. Furthermore, SG formation requires phosphorylation of eIF2α at serine 51[7]. There are four known kinases that are responsible for the phosphorylation of eIF2α under stress conditions, including PKR-like ER kinase (PERK)[8], double-stranded RNA-dependent protein kinase (PKR)[9], heme-regulated eIF2α kinase (HRI)[10], and general control non-derepressible protein 2 (GCN2)[11], each is activated by a distinct stimulus. Phosphorylation of eIF2α at serine 51 by one or more of these kinases results in polysome disassembly and translation inhibition[12].

SGs have been linked to several neurodegenerative diseases including Alzheimer's disease (AD)[13,14]. AD is neuropathologically characterized by the accumulation of aggregated hyperphosphorylated tau and β-amyloid (Aβ) in the brain[15,16]. Among these two proteins, the involvement of Tau in SG formation has already been established. Specifically, SGs core-nucleating protein TIA-1 is shown to bind to Tau, contributing to its aggregation and Tau-related neurodegeneration[17]. Tau inclusions in frontotemporal dementia with parkinsonism-17 (FTDP-17) and AD have been shown to colocalize with SGs, and these structures may increase tau deposition[18]. Mouse studies also revealed that the overexpression of Tau promotes and stabilizes SG formation in TIA-1 dependent manner[19]. Accumulation of TDP-43 inclusions in amyotrophic lateral sclerosis (ALS) and FTLD has been shown to be associated with SGs[18].

While tau has been linked to SG formation, the role of Aβ remains unknown. Understanding the role of Aβ in SG formation is crucial, given its importance in AD pathogenesis. Aβ, a 40–42 amino acid peptide, is crucial to the etiology of Alzheimer's disease. Native Aβ peptides undergo spontaneous structural changes, resulting in misfolded intermediates with β-sheets[20]. These intermediates are often unstable and subsequently aggregate to produce higher-order oligomers, protofibrils, and fibrils. Aβ is a widely recognized stressor and neurotoxin. Aβ

[1]Department of Cellular and Molecular Medicine, College of Medicine, Chosun University, Gwangju 61452, Republic of Korea. [2]Department of Biomedical Sciences, Chonnam National University, Gwangju, Republic of Korea. [3]Department of Animal Science, College of Agriculture and Life Sciences, Chonnam National University, Gwangju 61186, Republic of Korea. ✉email: vijaysankarr@gmail.com; tohn@chosun.ac.kr

has been shown to activate multiple stress signaling pathways, including endoplasmic reticulum[21] and oxidative stress[22]. However, the stress-inducing property on SG formation is unknown.

In this study, we explored the capacity of Aβ42 to induce SG and the associated molecular pathways in neuroblastoma-derived (SH-SY5Y) and glioma-derived (U87) cell lines. We found that the application of 20 μM Aβ42 resulted in the induction of approximately 30% SG formation within the treated cell lines. Given that our primary objective is to identify the molecular mechanisms underlying this occurrence, we selected this concentration for our subsequent analyses. We also observed increase in phospho-eIF2α levels in these cell lines upon exposure to Aβ42. Subsequently, through the application of stress kinase knockout cell lines and PLA analysis, we demonstrated that the activation of stress granules (SG) induced by Aβ42 is dependent on the protein kinase PKR.

Results

Aβ42 induced SGs in a cell-type specific manner

To determine the impact of Aβ42 exposure on SG formation, we subjected neuroblastoma- derived SH-SY5Y cells to varying concentrations of Aβ42 for 24 h. Following treatment, SG markers G3BP1 and eIF3b were used to immunostained the cells. Immunofluorescence (IF) analysis revealed that when exposed to concentrations of Aβ42 ranging from 20 and 40 μM, 20–30% of cells formed SGs enriched with SG markers G3BP1 and eIF3b (Fig. 1a,b). In our following experiments, we employed a concentration of 20 μM due to its consistency and optimal capacity in SG induction. Subsequently, HeLa, U2OS, U87, HEK, and HAP-1 cell lines were treated with 20 μM Aβ42 under identical experimental conditions to determine if Aβ42 could cause SG formation in these cell lines. Only U87 and HAP-1 cell lines showed significant SG formation in response to Aβ42 exposure, with the other cell lines displaying resistance (Fig. 2a and b). We then examined the phospho-eIF2α (S51) levels in these Aβ42-responsive cell lines. Immunoblot analysis of Aβ42-treated cell extracts revealed slightly higher phospho-eIF2α levels compared to the untreated control cells (Fig. 2c). These results suggest that Aβ42 causes SG formation in a cell type-specific manner and it depends on eIF2α phosphorylation.

Under stress conditions, global inhibition of protein synthesis is a common response[23,24]. To evaluate the influence of eIF2α phosphorylation induced by Aβ42 on global protein translation, puromycin (Tyr-tRNA mimetic) was employed to examine translation inhibition in SH-SY5Y and U87 cells post Aβ42 treatment. Subsequent immunoblotting of cell extracts using a puromycin antibody showed that treatment with Aβ42 did not lead to a significant alteration in overall protein translation in the treated cell lines (Fig. 2d). Following this, we carried out similar experiments with the reverse-Aβ42 peptide (reverse sequence of the wild type Aβ42 peptide, a kind gift from Prof. Park IL Seon, Chosun University) to investigate whether the formation of stress granules and the increase in phospho-eIF2α levels are specific to Aβ42. SH-SY5Y cells were treated with 20 μM reverse-Aβ42 for 24 h, after which we evaluated SG formation and the levels of p-eIF2α. However, the results from both immunocytochemistry (ICC) and immunoblotting demonstrated no SG formation and no changes

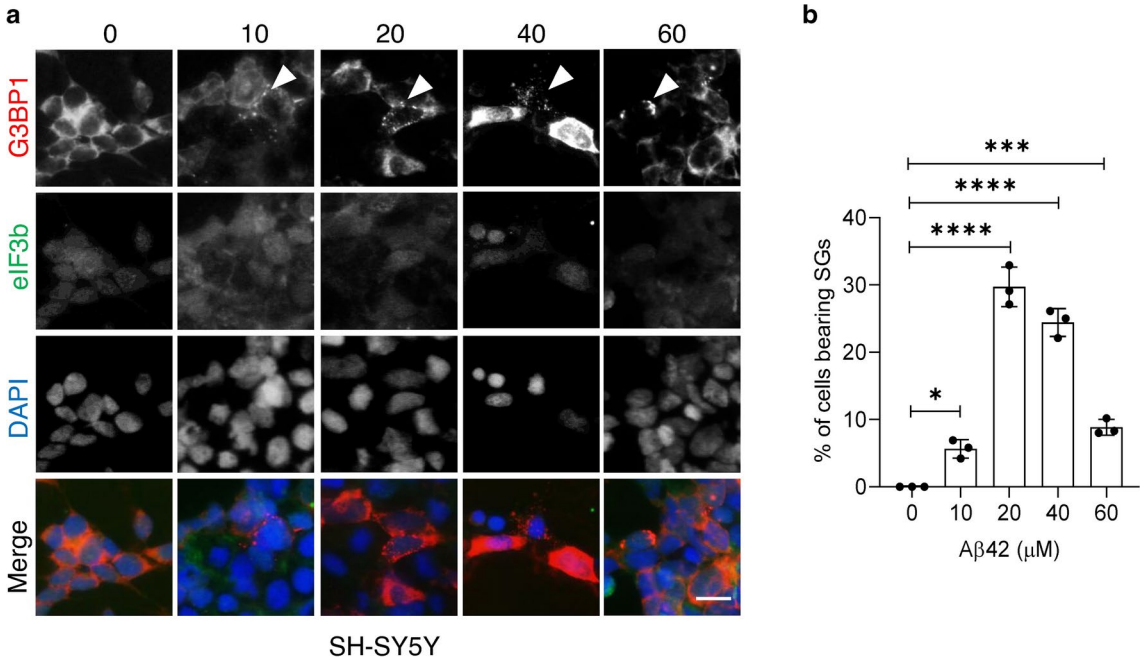

Fig. 1. Aβ42 exposure induced SG formation in SH-SY5Y cells. (**a**) cells were treated with indicated concentrations of Aβ42 for 24 h and then immunostained with SG markers eIF3b (green), G3BP1 (red), and nuclei stain DAPI (blue). Scale bar, 10 μm. (**b**) SG quantification data showing the percentage of cells harboring SGs. one-way analysis of variance (ANOVA) at the 95% confidence interval followed by a Dunnett's *post-hoc* test. Error bars indicate standard deviation (S.D.) (n = 3). $^{**}p < 0.01$, $^{***}p < 0.001$, $^{****}p < 0.0001$.

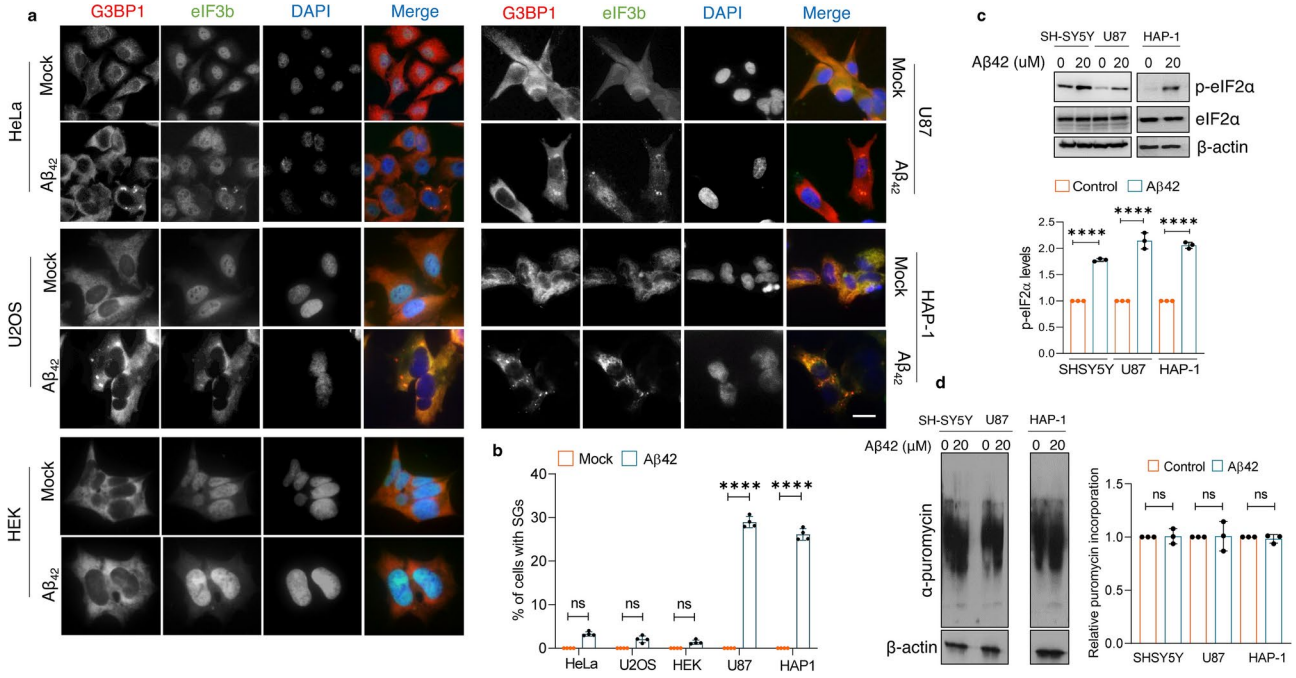

Fig. 2. Aβ42 exposure increased p-eIF2α levels but has no significant effect on global protein translation. (**a**) HeLa, U2OS, HEK, U87, and HAP-1 cell lines were seeded on coverslips with appropriate media in 4-well plates, grown and treated with 20 μM Aβ42 for 24 h. After that, cells were immunostained with eIF3b (green), G3BP1 (red) and nuclei stain DAPI (blue). Scale bar, 10 μm. (**b**) Bar graph shows the percentage of cells containing SGs. (one-way ANOVA at the 95% confidence interval followed by Bonferroni's *post-hoc* test, $^{****}P < 0.001$) Error bars indicate S.D. (n = 3), (**c**) Representative image of immunoblots and quantitative analysis showing the expression levels of p-eIF2α and eIF2α in Aβ42 treated cell lines. U87, SH-SY5Y, and HAP-1 cells were exposed to 20 μM Aβ42 for 24 h and the whole cell lysates were subjected to immunoblot. (one-way ANOVA, $^{****}p < 0.0001$) (**d**) Representative image of immunoblots and quantitative analysis showing the levels of puromycylated proteins under Aβ42 treatment. U87, SH-SY5Y, and HAP-1 cells were exposed to 20 μM Aβ42 followed by 10 min puromycin pulse (10 mg/ml) and the whole cell lysates were subjected to immunoblot (one-way ANOVA, ns).

in p-eIF2α levels (supplementary Fig. 1). These results imply that the processes of SG formation and eIF2α phosphorylation are specific to the wild-type Aβ42 sequence.

Monomeric and oligomeric Aβ42 exhibit superior SG-inducing properties

Aβ42 displays distinct conformations owing to its hydrophobic properties. We decided to investigate if these structural differences have any bearing on Aβ42's ability to induce SG. To achieve this, we exposed SH-SY5Y and U87 cells to 20 μM mono, oligo, and fibrillar Aβ42 for 24 h, and then we immunostained the cells using the SG markers G3BP1 and eIF3b. About 25% of the SH-SY5Y cells treated with monomeric Aβ42 had SGs. A similar pattern was observed with oligomeric Aβ42 treatment, with 20% of cells containing SGs. Conversely, SGs were found in only 3% of cells treated with fibrillar Aβ42 (Fig. 3a,b). A comparable pattern was observed when Aβ42 was applied to U87 cells (Fig. 3d,e). The results of the immunoblot analysis also indicated that p-eIF2α levels significantly raised by monomeric- Aβ42 compared to oligo-, and fibrillar-Aβ42 in these cell lines. Total eIF2α levels were unchanged. These findings indicate that the ability to induce SGs varies among different Aβ42 conformations.

Dutch and Flemish Aβ42 mutants induce SG formation

After examining the effect of Aβ42 structural variants on SG formation, we proceeded to examine the influence of Aβ42 familial Alzheimer disease (FAD) mutants on their SG induction characteristics. Although numerous FAD mutants have been reported, we have chosen the Dutch (E22Q) and Flemish (A21G) mutants for this investigation because of its altered aggregating properties; with the Dutch Aβ42 (Du-Aβ42) aggregating more quickly and the Flemish Aβ42 (Fl-Aβ42) aggregating more slowly than the wild type[25]. Du- and Fl-Aβ42 mutants were recombinantly expressed and purified as described previously[26]. After being exposed to 20 μM of Du- and Fl-Aβ42 for 24 h, SH-SY5Y and U87 cells were immunostained for the SG markers G3BP1 and eIF3b. Both familial mutant forms caused SG formation in these cell lines, according to IF image analysis (Fig. 4a and d). It's interesting to note that, in comparison to the Du-form, the Fl-Aβ42 caused SGs to increase two-fold in both SH-SY5Y and U87 cell lines (Fig. 4b and e). In these cell lines, Du-Aβ42 treatment induced 10% of SGs, while Fl-Aβ42 induced up to 20% under the same conditions. Additionally, Fl-Aβ42 treated cells had relatively higher phospho-eIF2α levels than Dutch mutant treated cells (Fig. 4c and f). Du-Aβ42 mutant exposed cells exhibit

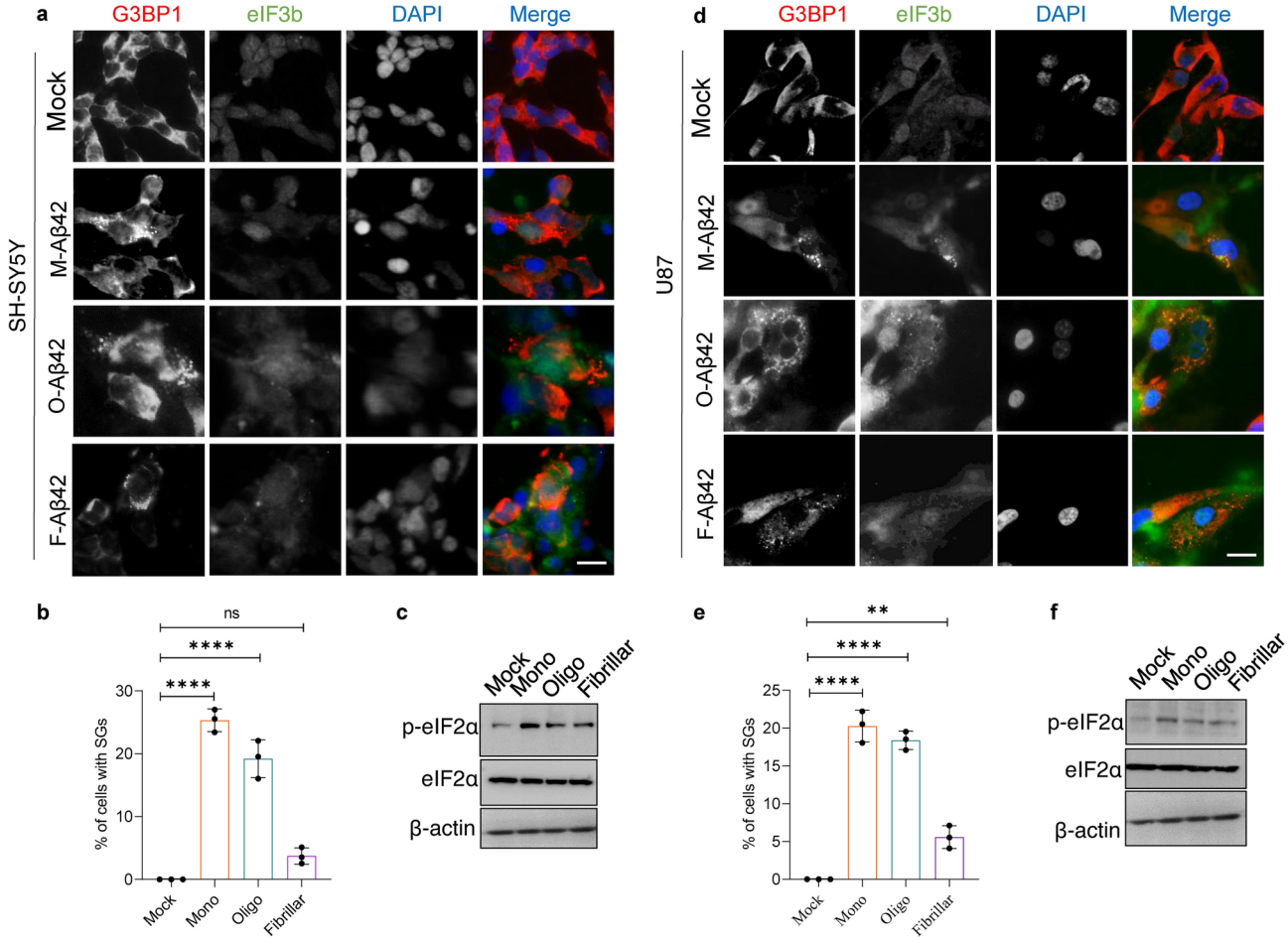

Fig. 3. Monomeric and oligomeric Aβ42 display better SG- inducing characteristics. (**a**) Representative images of G3BP1 and eIF3b immunofluorescence staining of SH-SY5Y cells treated with different conformers of Aβ42. Scale bar, 10 µm. (**b**) Bar graph shows the percentage of cells containing SGs. one-way ANOVA at the 95% confidence interval followed by Dunnett's *post-hoc* test, $^{****}p < 0.0001$. Error bars indicate S.D. (n = 3), (**c**) Representative image of immunoblots showing amount of p-eIF2α in Aβ42 treated SH-SY5Y cells. (**d**) Representative images of G3BP1 and eIF3b immunofluorescence staining of U87 cells treated with different conformers of Aβ42. Scale bar, 10 µm. (**e**) Bar graph shows the percentage of cells containing SGs. one-way ANOVA at the 95% confidence interval followed by Dunnett's *post-hoc* test, $^{**}p < 0.01$, $^{***}p < 0.001$, $^{****}p < 0.0001$. Error bars indicates S.D. (n = 3) (**f**) Representative image of immunoblots showing expression level of p-eIF2α and eIF2α in Aβ42 treated U87 cells.

lesser SG formation and eIF2α phosphorylation. These findings imply that, in comparison to the Dutch mutant, the Flemish mutant possesses a notable SG-inducing characteristic.

Aβ42-induced SG formation requires PKR kinase

Next, we tested which stress kinase is activated to promote SG assembly upon Aβ42 stress. To identify this, we used the wild-type HAP-1 cell line along with four eIF2a kinases knockout such as HRI, PKR, PERK, and GCN2. Our early experiment (Fig. 2a and b) showed that Aβ42-induced SG formation in these cell lines corresponded to that of SH-SY5Y cells. Therefore, we selected these knockout cell lines for this experiment, HAP1 knockouts were generated from the HAP-1(C631) parental cell line by employing the CRISPR-Cas9 system by Horizon Discovery, resulting in the incorporation of frameshift mutations into the coding sequences of designated genes: HRI, PKR, PERK, and GCN2. Before commencing the experiment, we chose to validate the knockout (KO) levels of the specified proteins in the aforementioned cell lines. Both HAP-1 wild type and KO cell lines were harvested, and the total cell lysate was analyzed via immunoblotting. Immunoblotting results confirmed the KO status of the targeted protein levels in the respective cell lines compared to the wild type HAP-1 cells (Fig. 3a). Later, these knockout cells were treated with 20 µM Aβ42 for 24 h and then immunostained with SG marker protein G3BP1 and eIF3b. The results showed approximately 20% WT HAP-1 cells with SGs as observed earlier in this study. On the other hand, all KO cells produced significantly lower SGs than the WT cells under Aβ42 treatment. Among these cell lines, the PKR-KO cell line showed a significant decrease in SG bearing cells. These data demonstrate that Aβ42 induces SGs in a PKR kinase-dependent manner (Fig. 5a,b).

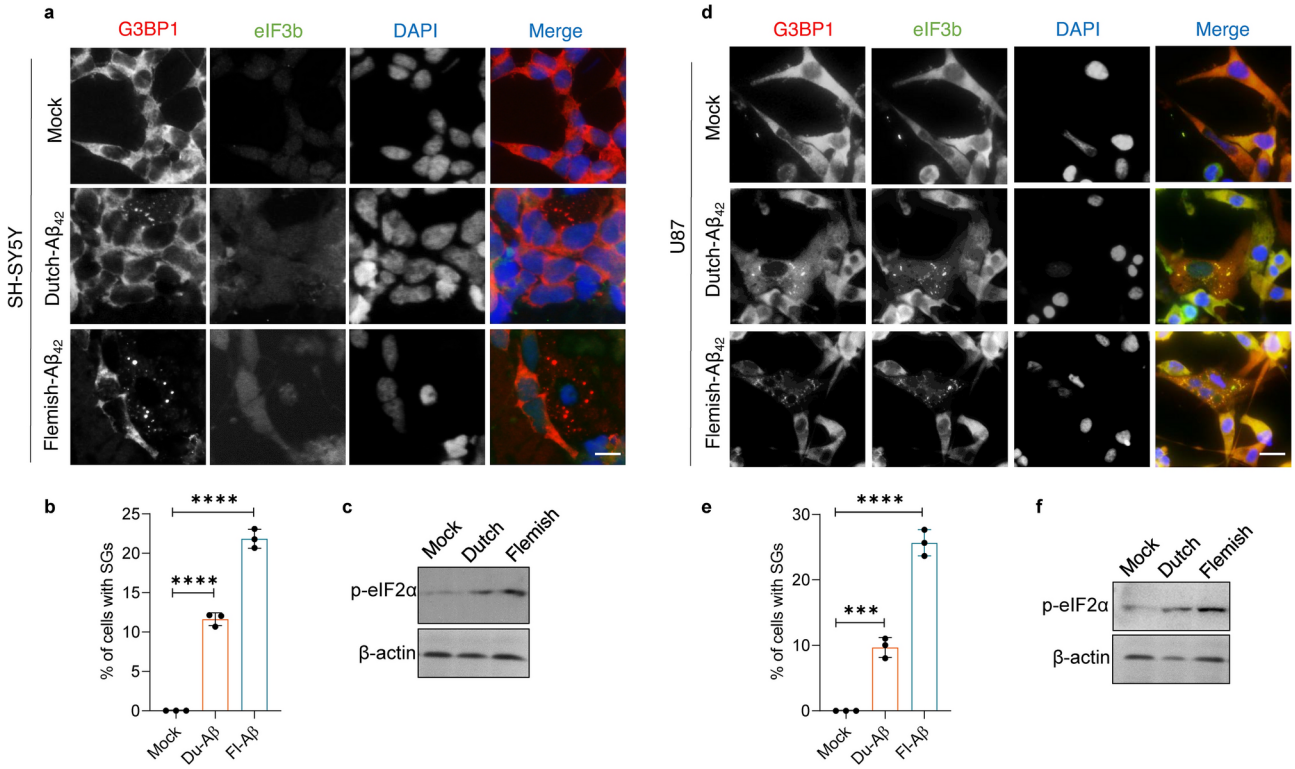

Fig. 4. Dutch- and Flemish-Aβ42 display distinct SG- inducing characteristic. (**a**) Representative images of G3BP1 and eIF3b immunofluorescence staining of SH-SY5Y cells treated with Du- and Fl-Aβ42 for 24 h. Scale bar, 10 µm. (**b**) Bar graph shows the percentage of cells containing SGs. one-way ANOVA at the 95% confidence interval followed by Dunnett's *post-hoc* test, $^{****}p < 0.0001$. Error bars indicate S.D. (n = 3), (**c**) Representative image of immunoblots showing amount of p-eIF2α and eIF2α in Du- and Fl-Aβ42 treated SH-SY5Y cells. (**d**) Representative images of G3BP1 and eIF3b immunofluorescence staining of U87 cells treated with Du- and Fl-Aβ42. (**e**) Bar graph shows the percentage of cells containing SGs. one-way ANOVA at the 95% confidence interval with Dunnett's *post-hoc* test, $^{***}p < 0.001$, $^{****}p < 0.0001$. Error bars indicate S.D. (n = 3). (**f**) Representative image of immunoblots showing amount of p-eIF2α in Du- and Fl-Aβ42 treated U87 cells.

Following this, we conducted a similar experiment with Du- and Fl-Aβ42 in these KO cell lines because Fl-Aβ42 demonstrated a level of SG-inducing property comparable to WT-Aβ42. Exposure to Fl-Aβ42 resulted in significantly increased SG formation in HAP-1 WT cells compared with Du- Aβ42 as observed earlier in this study. On the other hand, when exposed to Fl-Aβ42, HAP-1 KO cells displayed less SG formation than HAP-1 WT cells. Additionally, a notable drop in SG-bearing cells was observed in the PKR-KO cell line. Similar pattern of SG formation in HAP-1 KO cells has been observed with Du- Aβ42 (Fig. 6a,b). When combined, our findings imply that SGs are induced by WT- and familial- Aβ42 mutants in a way that is PKR kinase-dependent.

Aβ42 exposure facilitates PACT-PKR interaction

Our results suggest the role of PKR kinase in Aβ42-induced SG formation. Nevertheless, the mechanism through which Aβ42 triggers the activation of PKR remains unclear within this framework. PKR is activated primarily by a double-stranded RNA during viral infection. It was also later shown to be activated in response to oxidative stress[27], and endoplasmic reticulum stress[28]. While double-stranded RNA can bind to PKR and activate it directly. Activation of PKR in response to several other stressors depends on its interaction with a cellular protein, protein activator of PKR (PACT)[29]. Therefore, in our next experiment, we decided to test whether Aβ42 exposure induces the PACT: PKR interaction. We performed in-situ proximity ligation (PLA) assay to analyze this interaction in SH-SY5Y and U87 cell lines after Aβ42 exposure. The results showed positive PLA amplicon signals (red) in approximately 20–30% of cells treated with Aβ42 for 24 h in both cell lines compared to the control (Fig. 7a,b).

We next performed PLA assay to evaluate the PACT/PKR interaction in AD transgenic mouse hippocampus. 6 months old 5XFAD transgenic mice and age-matched wild type (C57BL/6J) control mice hippocampal slices were subjected for PLA analysis with PACT/PKR antibodies. Slices treated with primary antibodies only (without PLA probes) used as a control. We observed the presence of PLA-positive complexes of different sizes, from small to large ones (Fig. 7c, arrow heads) in 5XFAD mouse hippocampus. The findings from the PLA indicate that PACT is either co-localized with PKR or situated in close proximity, which implies a possible involvement

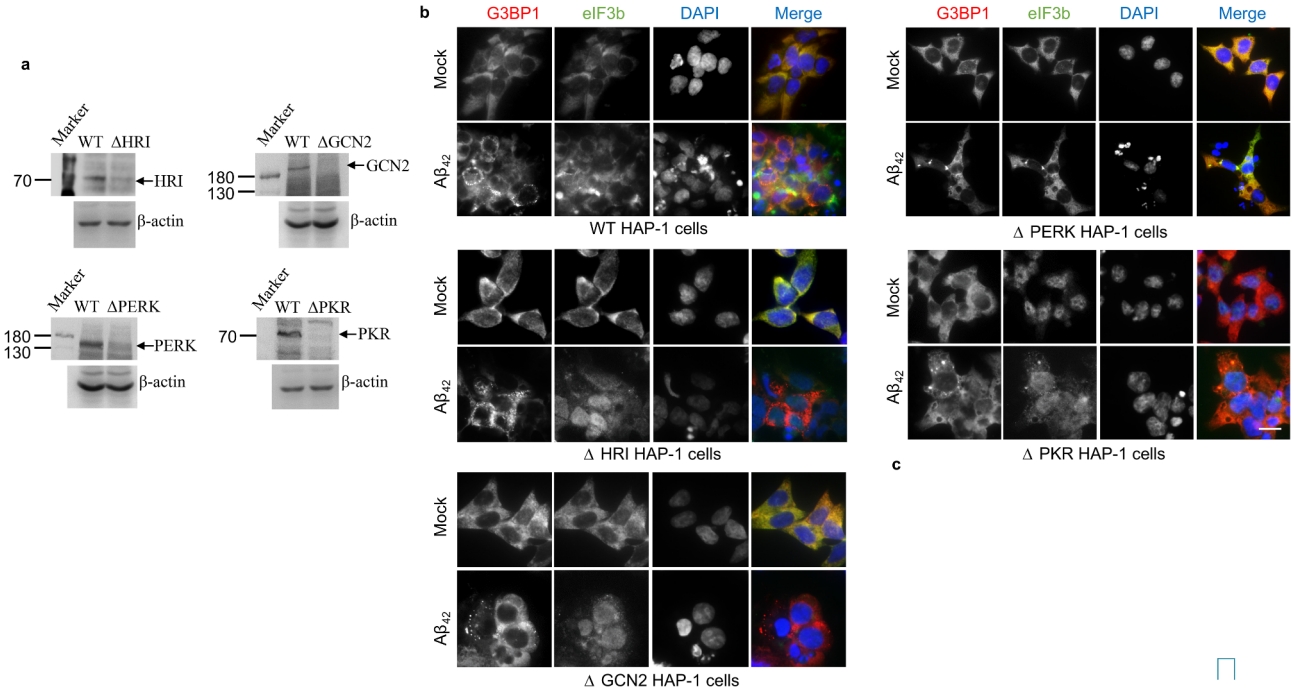

Fig. 5. Aβ42 induced SG formation is PKR-dependent. (**a**) Immunoblot analysis of HRI, GCN2, PERK, and PKR protein expression levels in HAP-1 WT and KO cell lines. Whole cell lysates of HAP-1 WT and KO cell lines were subjected to immunoblot with respective antibodies (**b**) Representative images of G3BP1 and eIF3b immunofluorescence staining of HAP-1-WT and -KO cells treated with Aβ42. Scale bar, 10 µm. (**c**) Bar graph shows the percentage of cells containing SGs. one-way ANOVA with Bonferroni's post-hoc test, $^{*}p < 0.05$, $^{****}p < 0.0001$. Error bars indicate S.D. (n = 3).

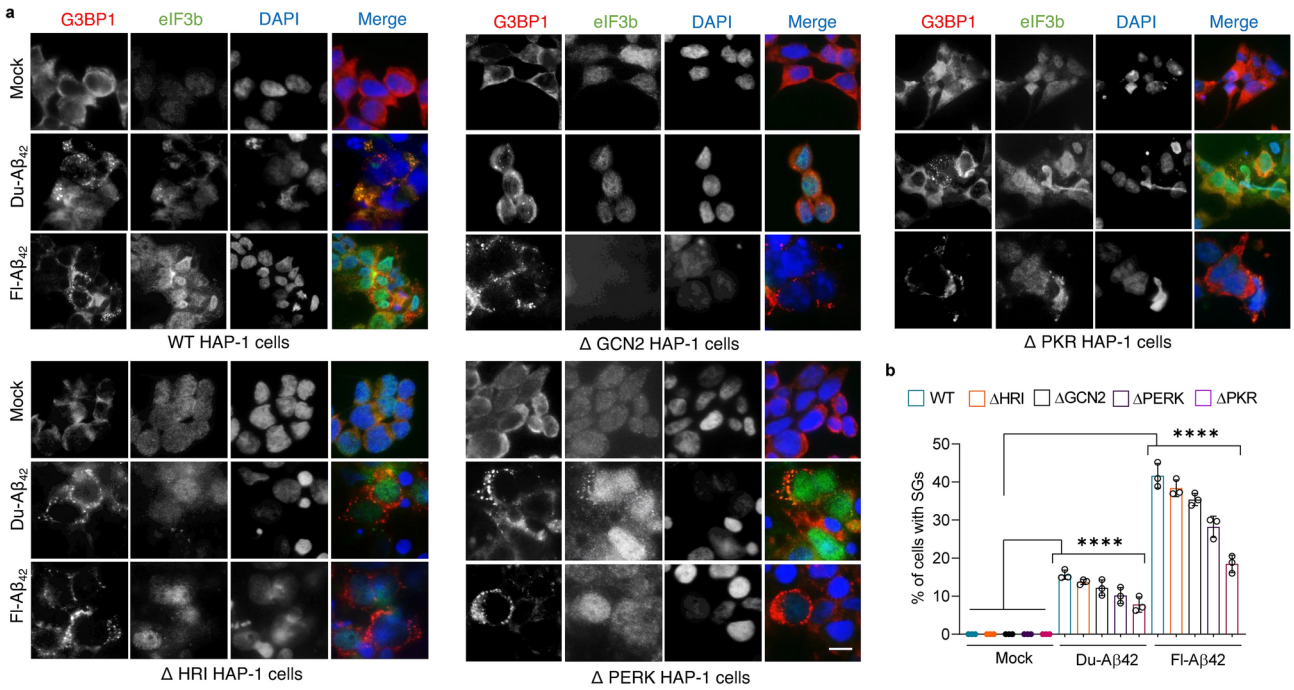

Fig. 6. Du- and Fl-Aβ42 induced SG formation is PKR-dependent. (**a**) Representative images of G3BP1 and eIF3b immunofluorescence staining of HAP-1-WT and -KO cells treated with Du- and Fl-Aβ42 for 24 h. Scale bar, 10 µm. (**b**) Bar graph shows the percentage of cells containing SGs. one-way ANOVA at the 95% confidence interval with Bonferroni's post-hoc test, $^{****}p < 0.0001$. Error bars indicate S.D. (n = 3).

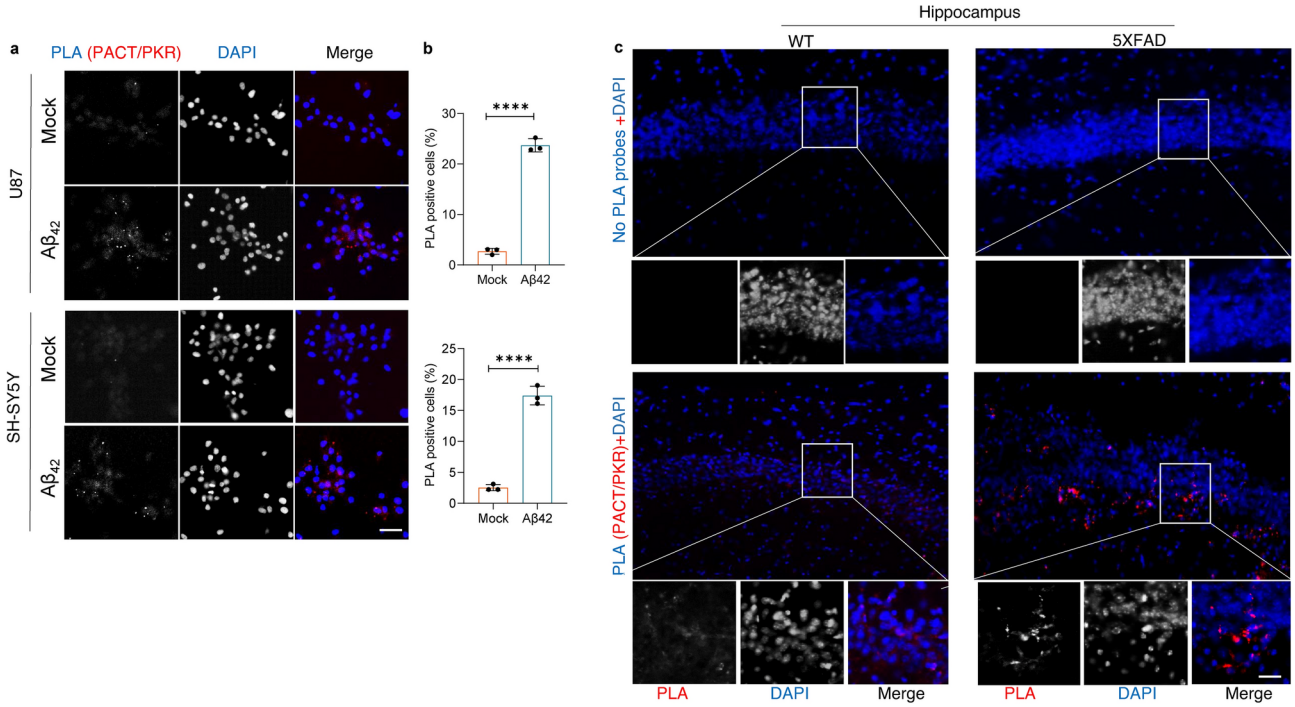

Fig. 7. Aβ42 induced SG formation requires PACT: PKR interaction. (**a**) Representative images of PACT/PKR (red) proximity ligation assay of SH-SY5Y and U87 cells treated with Aβ42. Nuclei stained with DAPI (blue) Scale bar, 10 µm. (**b**) Bar graph shows the percentage of PACT/PKR positive cells. Two-tailed T-test, $^{****}P < 0.0001$ Error bars indicate S.D. (n = 2), (**c**) Representative Images of PACT/PKR (red) proximity ligation assay of wild type and 5XFAD mouse hippocampus. Nuclei stained with DAPI (blue). Scale bar, 50 µm.

of PACT in the activation of PKR. Overall, our results suggest that PKR kinase is the primary mediator of Aβ42-induced SG formation.

Discussion

In this study, we investigated the SG-inducing properties of Aβ42 in cultured cell lines. Aβ42 exposure results in SG formation and increased eIF2α phosphorylation in neuroblastoma-derived (SH-SY5Y) and glioma-derived (U87) cell lines. Non-neuronal cell lines were less responsive to Aβ42 mediated SG formation. We also observed that different structural variants and familial mutants of Aβ42 exhibited varying levels of SG formation in these cell lines. By treating the stress kinases knockout (KO) cells with Aβ42, we discovered that Aβ42 primarily induces SG formation through the PKR kinase. Furthermore, we confirmed that the interaction of PACT with PKR are crucial for Aβ42-mediated SG formation.

Many neurodegeneration-associated proteins have been shown to interact and facilitate SG formation. For example, in Huntingtin disease, expanded Htt shifts to SGs and establishes interactions with G3BP1 and Caprin1 upon ER stress[30]. In AD, tau interaction with SGs has crucial implications for tauopathies pathogenesis because it promotes the production of insoluble tau aggregates[19]. In the present study, we demonstrated that exposure to Aβ42 for 24 h triggered stress granule formation in both neuroblastoma-derived (SH-SY5Y) and glioma-derived (U87) cell lines. Initially, SH-SY5Y cells were exposed to different concentrations for 24 h, with 20 and 40 uM concentrations leading to significant stress granule formation. We noticed reduction in SG formation with increasing concentrations of Aβ42, we speculate that this could be due to loss of cell viability at higher concentrations in these cell lines. Subsequently, cells were treated with a fixed concentration of 20 uM at various time intervals (6, 12, 24, and 36 h). Stress granule formation was significant only at the 24-h time point, with no granules observed at 6 and 12 h. At 36 h, some stress granule formation was noted, but it was considerably lower than at 24 h (Data not shown). To elucidate the molecular mechanism of Aβ42-induced SG formation, we sought a concentration that would induce 30–50% of SG formation in these cell lines and observed 20 µM concentration led to a maximum of 28% of cells exhibiting this phenomenon. Based on these findings, the 20 µM concentration and 24-h time point were chosen for subsequent experiments.

Based on this observation, we conducted an analysis of the p-eIF2α levels and global protein translation under these conditions. In response to various stress stimuli, the α subunit of eIF2 is typically phosphorylated at Ser51, leading to the inhibition of general translation initiation[31]. Consistent with these findings, our study revealed elevated levels of eIF2α phosphorylation in cells exposed to Aβ42. However, our findings indicate that there was no significant change in global translation inhibition after Aβ42 treatment. This lack of change could be attributed to the fact that only 20% of cells formed SGs when exposed to Aβ42, suggesting a weaker stress intensity that does not affect global protein translation. Similar observation has been documented in an

animal study where an increased level of hippocampal PKR-dependent eIF2α phosphorylation has been found to significantly impair memory consolidation, regardless of any global alterations in protein synthesis[32].

Due to its aggregative nature, Aβ exhibits various structural variants, and these structural variations are highly correlated with its levels of cytotoxicity. The three main structural variations are mono, oligo, and fibrils; of these, oligomeric Aβ42 has been shown to be extremely cytotoxic[33–35]. In this study, we have observed that all structural forms of Aβ42 have the ability to induce the formation of SGs. However, it was noted that cells exposed to the monomeric and oligomeric forms exhibited a significantly higher level of SG formation compared to the cells treated with the fibrillar form. A separate study conducted on mouse cell lines also reported the occurrence of SG formation induced by both soluble and fibrillar Aβ after a 24-h exposure[36]. Our study yielded similar results to this previous research. Nevertheless, the underlying reasons for the variation in SG induction by these different structural variants remain unclear. One plausible explanation could be the formation of toxic intermediates. These transient structures are more likely to occur with the monomeric and oligomeric states of Aβ. In contrast, the fibrillar form of Aβ, being already in an aggregated state, has limited potential for the formation of such transient structures. Previous studies have shown that exposure to either structural form of Aβ42 elevated levels of p-eIF2α[37]. In our study, we observed the Aβ42 structural variants displayed variation in eIF2α phosphorylation levels.

Following this, we have observed a similar pattern of SG induction by the FAD Aβ42 mutants in the aforementioned cell lines. Among the FAD mutants of Aβ, Dutch (E22Q) and Flemish (A21G) have been extensively studied. Both forms of Aβ42 have been thoroughly characterized in both in vitro[25] and in vivo[38] settings. In vitro studies have demonstrated that the Dutch mutant exhibits a higher propensity for nucleation and fibrillation compared to the wild type, while the Flemish mutant shows a significantly reduced rate of fibril formation. Our data from ICC imaging and Western blot analysis indicate that the Flemish variant displays more pronounced SG-inducing characteristics compared to the Dutch variant. We propose that this discrepancy may be attributed to the altered aggregating properties of Aβ, with the Dutch variant aggregating more rapidly and the Flemish variant aggregating more slowly than the wild type. This suggests the aggregation property influenced by the familial mutations correlate with these Aβ neurotoxicity. Based on these findings, we put forward the hypothesis that the slower and more stable formation of soluble oligomeric or other early toxic Aβ intermediates by the Flemish variant may underlie this phenomenon.

Various stress-related signaling pathways have been demonstrated to react to neurotoxicity in AD. Oxidative stress markers[39], ER stress[40], and stress kinases are present at abnormally high levels in AD brains[41–44]. Exposure to Aβ42 peptides has been proven to stimulate oxidative, endoplasmic reticulum, and unfolded protein response stress signaling pathways both in cultured cells and AD brain[45,46]. In this investigation utilizing HAP-1 KO cell lines of diverse stress kinases, it is demonstrated that both WT- and Fl-Aβ42 exposure induced SG formation in all KO cell lines. However, a notable reduction in SG formation was observed in PKR KO cells. Furthermore, relatively similar levels of SG formation were observed in both WT and HRI KO cells, indicating the minimal involvement of this kinase in Aβ42-induced SG formation. These findings suggest the significant role of PKR kinase in the Aβ42-induced stress mechanism. Previous research has also indicated that Aβ42 activates neuronal PKR in vitro and in vivo to enhance p-eIF2α levels[37,47]. Our outcomes supported a similar scenario where p-eIF2α levels, influenced by PKR and other kinases, are crucial for Aβ42-mediated SG formation.

Protein kinase R (PKR) is a widely distributed serine-threonine kinase that can be primarily activated by double-stranded RNA (dsRNA) from viruses. In the absence of viral infection, PKR can also be activated by PACT protein. In AD brains, activated PKR has been detected in neuronal cytoplasm, granulo-vacuolar degeneration, neuronal nuclei, and around senile plaques[48]. In cell cultures, both PKR and PACT can be activated by the Aβ peptide[49]. Our findings further support this by demonstrating an increase in PACT-PKR colocalization following exposure to Aβ42 in SH-SY5Y and U87 cell lines using the PLA method. Also, PLA results from transgenic mice (5XFAD) hippocampus shown increased PACT/PKR PLA signals suggesting their possible interaction in AD condition. Together, these results suggest the involvement of PACT in Aβ42-mediated stress granule (SG) formation.

In conclusion, the findings outlined in this study shed light on the process by which Aβ42 influences SG formation. It was demonstrated that Aβ42 triggers eIF2α phosphorylation and subsequently induces SG formation through the activation of the PACT/PKR pathway. Our current research represents a preliminary examination of the SG-inducing pathways that could be influenced by Aβ42, establishing crucial groundwork for future inquiries. Additionally, it emphasizes the importance of conducting further investigations to better understand the effects of clinically significant levels of Aβ42 on these mechanisms in primary neuronal cell cultures and neural tissue derived from living brains.

Materials and methods

Cell culture and reagents

SH-SY5Y (American type culture collection, CRL-2266), U87 (ATCC, HTB-14), HeLa (ATCC, CCL-2), U2OS (ATCC, HTB-96), HEK293(ATCC, CRL-1573) cells were obtained from ATCC. All cell lines were grown in DMEM medium (Welgene) that was supplemented with 10% heat-inactivated fetal bovine serum (Welgene) and 1% (v/v) penicillin and streptomycin (Lonza). HAP-1 (horizon, C631) cells were procured from Horizon Discovery. HAP1 knockouts were generated from the HAP-1(C631) parental cell line by employing the CRISPR-Cas9 system by Horizon Discovery, resulting in the incorporation of frameshift mutations into the coding sequences of designated genes: ΔHRI (HZGHC000141c006), ΔPKR(HZGHC000338c010), ΔPERK(HZGHC003428c002), and ΔGCN2 (HZGHC002987c010). HAP1 cells were cultured in IMDM, that was supplemented with 10% heat-inactivated fetal bovine serum (Welgene) and 1% (v/v) penicillin and streptomycin (Lonza). The cultures were maintained at 37 °C in an atmosphere containing 5% CO_2.

Puromycin Dihydrochloride were obtained from Sigma. The following antibodies have been used in this study. Anti-eIF3b (N-20) [sc-16377], Anti-G3BP1 (H-10) [sc-365338], eIF2α (FL-315) [sc-11386], HRI (D12) [sc-365239] and, PKR (A12) [sc-393038] were ordered from Santa Cruz Biotechnology. Anti-Aβ42 (6E10) [SIG-39300] was from Covance. Anti-phospho-eIF2α (BML-SA405) was purchased from Enzo Life Sciences, Anti-Puromycin 12D10 [MABE343] antibody was purchased from EMD Millipore, β-actin (AC-15) [ab6276] was obtained from Abcam. GCN2 [3302S], PACT(D9N6J) [13490S] and, PERK (C33E10) [3192S] from Cell signaling. All secondary antibodies used in immunoblot or immunofluorescence microscopy including HRP (Horseradish peroxide conjugated) or Cy2/Cy3, were from Jackson Immunoresearch Laboratory.

Mice

5XFAD (APP KM670/671NL [Swedish], APP I716V [Florida], APP V717I [London], PSEN1 M146L, PSEN1 L286V, 5–6 months old, Jackson Laboratory) and Wild-type (C57BL/6J, 5–6 months old) mice were used for the experiments. All the animals were caged individually with free access for the food and water.

Preparation of Aβ42

All forms of Aβ42 peptides were expressed in E. coli as fusion proteins and purified as previously described[26]. Purified peptides were solubilized in 100% 1,1,1,3,3,3-hexafluoro-2-propanol, and dried initially under nitrogen and then under vacuum for 30 min. Purified Aβ42 peptides were further verified with Aβ42 (6E10) antibody using immunoblot (supplementary Fig. 2a). Fibrillogenic properties of purified Aβ42 peptides were analyzed by Thioflavin-T (Th-T) assay (supplementary Fig. 2b). Amyloid-β peptides were dissolved in PBS (300 µl) and allowed to aggregate at 37 °C for the indicated times without shaking, and 20 µl of these mixtures were then mixed with 80 µl of 5 µM Th-T in PBS solution. Fluorescence were measured immediately at excitation and emission wavelengths of 445 and 490 nm, respectively, using a microplate spectrofluorometer (Gemini-XS; Molecular Devices, Sunnyvale, CA, USA).

Peptide aliquots were stored at − 20 °C until required. Immediately before use, peptides were dissolved in 0.1% NH4OH at a concentration of 2 mg/ml and sonicated for 10 min at 4 °C. Solutions were diluted to the desired concentrations with PBS or culture media. For the treatment of cell cultures, the peptide solution was diluted to the specified concentrations with the appropriate cell culture media. The control group (mock) was administered culture media and a volume equivalent to 0.1% NH4OH in the Aβ42 treatment group, excluding the addition of Aβ42. Aβ42 oligomers and mature fibrils were prepared as previously described[50] with some modification. Briefly, for oligomers, freshly prepared peptides were diluted with cell culture media to 100 µM, vortexed for 30 s, incubated at 4 °C for 12 h, and then diluted to the desired concentrations. To make fibrils, Aβ42 (100 µM) was incubated in presence of 0.02% sodium azide in PBS at 37 °C for 4 days, centrifuged at 16,000 g for 30 min, and the pellets (fibrils) obtained were washed three times with PBS, and sonicated for 10 min. Fibrils were quantified using the Bradford method and used immediately by diluting them to the desired concentrations in culture media or stored at − 80 °C.

Immunoblot analysis

Cells were lysed with RIPA lysis buffer (Sigma, R0278) supplemented with Halt protease and phosphatase inhibitors (Thermo Scientific, 78,440) for 15 min in ice and centrifuged at 13,000 rpm for 15 min. Total proteins were quantified using Bradford reagent (Biorad). Total proteins (20–50 µg) subjected to 8–15% SDS-PAGE, transferred to PVDF membranes and probed with the indicated antibodies. Antibody detection was performed using Pico-EPD western blot detection kit (ELPIS-biotech).

Immunofluorescence analysis

Cells were grown on coverslips in 4-well plates. The next day, the cells were treated with Aβ42 for 24 h. After treatment, the cells on the coverslips were washed twice with PBS and fixed with 4% paraformaldehyde and permeabilized with ice-cold methanol for 10 min and blocked with 5% normal horse serum in PBS containing 0.02% sodium azide for 1 h at room temperature. All primary antibodies diluted in blocking solution were added to the cell and incubated overnight at 4 °C. Cells were washed with PBS (pH 7.4) for three time (10 min each), incubated with respected secondary antibodies for 1 h at RT, washed with PBS (pH 7.4) for three times. The fixed cells were then mounted on a glass slide with Fluoromount-G (Invitrogen) mounting medium containing DAPI. Fluorescence images were taken with the help of Nikon Eclipse 80i fluorescence microscope. ImageJ and Photoshop software were used for image arrangements.

Approximately 1000 cells were counted (distributed over 20 different randomly selected fields within each coverslip). Cells were counted manually, where a cell containing stress granules was identified as the one that has ≥3 distinct and clear granules. Those cells are scored positive cells, whereas others are scored negative. Moreover, we zoomed the image to be able to distinguish between cells during counting. In addition, dead cells or morphologically differentiated cells were excluded from the count. The percentages of cells with SGs were quantified by counting the positive cells over the total number of cells in 20 different independent fields. Data was calculated from three independent experiments and presented as mean ± S.D.

Ribopuromycylation assay

SH-SY5Y, U87 and HAP-1 cells were treated with 20 µM Aβ42 for 24 h, then pulsed with 10 mg/ml puromycin (Cayman Chemical) for 10 min at 37 °C in 5% CO_2 incubator except control. Then cells were washed with cold 1XPBS twice and lysed with RIPA lysis buffer. All proteins were subjected to western blot analysis. Puromycin antibody (1:15,000) used to detect against ribopuromycylated proteins.

In situ PLA

Following a 24-h treatment with Aβ42, SH-SY5Y and U87 cells were fixed using 4% paraformaldehyde and permeabilized with 0.1% Triton X-100. Subsequently, the cells were subjected to incubation with primary antibodies, followed by incubation with PLA probes (anti-mouse (Duo 92,002) and anti-rabbit (Duo92004) IgG antibodies conjugated with oligonucleotides), ligation, and amplification as per the manufacturer's guidelines (Duolink In Situ detection reagents, Sigma-Aldrich, duo92007). The primary antibodies utilized in this experiment were PACT antibody (cell signaling, 13,490) and PKR antibody (Santa Cruz Biotechnology, sc-393038). Imaging was performed using a Nikon Eclipse 80i fluorescence microscope. To determine the percentage of cells exhibiting at least one red fluorescent dot per cell, 100 cells were assessed per sample and experiment through microscopic analysis.

Tissue in situ PLA was performed as described earlier with minor modifications[51,52]. Briefly, 5XFAD and WT mice were sacrificed using cervical dislocation, followed by rapid removal of the brain and immersion in ice-cold 1XPBS. The hippocampi were extracted and fixed in 4% PFA overnight. Subsequently, the hippocampi were rinsed in 1XPBS, immersed in 10% sucrose overnight, and then in 30% sucrose overnight to minimize tissue damage during cryosectioning. The hippocampal tissue was embedded in O.C.T compound, sliced to a thickness of 50 µm using a Leica CM1860 tissue processor (Leica Biosystems, Germany), and mounted on glass slides. Sections were incubated in a blocking solution (provided by the kit) and the manufacturer's instructions was followed for the remaining steps. Imaging was conducted using a Nikon Eclipse 80i fluorescence microscope.

Statistics

Data analysis was performed in GraphPad Prism v 8. Data are presented as mean ± standard deviation unless otherwise stated. Comparison of means was performed using Student's t-test for two groups or one-way ANOVA for three or more groups followed by a Dunnett's multiple comparison test (comparison to one control group) or followed by a Bonferroni's multiple comparisons test (comparison among all groups) at the 95% confidence interval. Differences were declared statistically significant if $p < 0.05$, and the following statistical significance indicators are used: $^{*}p < 0.05$, $^{**}p < 0.01$, $^{***}p < 0.001$, $^{****}p < 0.0001$.

Data availability

The data sets generated and/or analysed during the present study are available from the corresponding author on reasonable request.

Received: 17 May 2024; Accepted: 28 January 2025
Published online: 18 February 2025

References

1. Palangi, F., Samuel, S. M., Thompson, I. R., Triggle, C. R. & Emara, M. M. Effects of oxidative and thermal stresses on stress granule formation in human induced pluripotent stem cells. *PLoS ONE* **12**, e0182059. https://doi.org/10.1371/journal.pone.0182059 (2017).
2. Sun, C. L., Van Gilst, M. & Crowder, C. M. Hypoxia-induced mitochondrial stress granules. *Cell Death Dis.* **14**, 448. https://doi.org/10.1038/s41419-023-05988-6 (2023).
3. Iadevaia, V. et al. Novel stress granule-like structures are induced via a paracrine mechanism during viral infection. *J. Cell Sci.* https://doi.org/10.1242/jcs.259194 (2022).
4. Protter, D. S. W. & Parker, R. Principles and properties of stress granules. *Trends Cell Biol.* **26**, 668–679. https://doi.org/10.1016/j.tcb.2016.05.004 (2016).
5. Gilks, N. et al. Stress granule assembly is mediated by prion-like aggregation of TIA-1. *Mol. Biol. Cell* **15**, 5383–5398. https://doi.org/10.1091/mbc.e04-08-0715 (2004).
6. Tourriere, H. et al. The RasGAP-associated endoribonuclease G3BP assembles stress granules. *J. Cell Biol.* **160**, 823–831. https://doi.org/10.1083/jcb.200212128 (2003).
7. Wek, R. C. Role of eIF2alpha kinases in translational control and adaptation to cellular stress. *Cold Spring Harb. Perspect. Biol.* https://doi.org/10.1101/cshperspect.a032870 (2018).
8. Harding, H. P., Zhang, Y., Bertolotti, A., Zeng, H. & Ron, D. Perk is essential for translational regulation and cell survival during the unfolded protein response. *Mol. Cell* **5**, 897–904. https://doi.org/10.1016/s1097-2765(00)80330-5 (2000).
9. Srivastava, S. P., Kumar, K. U. & Kaufman, R. J. Phosphorylation of eukaryotic translation initiation factor 2 mediates apoptosis in response to activation of the double-stranded RNA-dependent protein kinase. *J. Biol. Chem.* **273**, 2416–2423. https://doi.org/10.1074/jbc.273.4.2416 (1998).
10. McEwen, E. et al. Heme-regulated inhibitor kinase-mediated phosphorylation of eukaryotic translation initiation factor 2 inhibits translation, induces stress granule formation, and mediates survival upon arsenite exposure. *J. Biol. Chem.* **280**, 16925–16933. https://doi.org/10.1074/jbc.M412882200 (2005).
11. Wek, S. A., Zhu, S. & Wek, R. C. The histidyl-tRNA synthetase-related sequence in the eIF-2 alpha protein kinase GCN2 interacts with tRNA and is required for activation in response to starvation for different amino acids. *Mol. Cell Biol.* **15**, 4497–4506. https://doi.org/10.1128/MCB.15.8.4497 (1995).
12. Hofmann, S., Kedersha, N., Anderson, P. & Ivanov, P. Molecular mechanisms of stress granule assembly and disassembly. *Biochim. Biophys. Acta Mol. Cell Res.* **1868**, 118876. https://doi.org/10.1016/j.bbamcr.2020.118876 (2021).
13. Sato, K., Takayama, K. I. & Inoue, S. Stress granules sequester Alzheimer's disease-associated gene transcripts and regulate disease-related neuronal proteostasis. *Aging (Albany NY)* **15**, 3984–4011. https://doi.org/10.18632/aging.204737 (2023).
14. Ash, P. E., Vanderweyde, T. E., Youmans, K. L., Apicco, D. J. & Wolozin, B. Pathological stress granules in Alzheimer's disease. *Brain Res.* **1584**, 52–58. https://doi.org/10.1016/j.brainres.2014.05.052 (2014).
15. Gu, J. L. & Liu, F. Tau in Alzheimer's disease: Pathological alterations and an attractive therapeutic target. *Curr. Med. Sci.* **40**, 1009–1021. https://doi.org/10.1007/s11596-020-2282-1 (2020).
16. Busche, M. A. & Hyman, B. T. Synergy between amyloid-beta and tau in Alzheimer's disease. *Nat. Neurosci.* **23**, 1183–1193. https://doi.org/10.1038/s41593-020-0687-6 (2020).
17. Vanderweyde, T. et al. Contrasting pathology of the stress granule proteins TIA-1 and G3BP in tauopathies. *J. Neurosci.* **32**, 8270–8283. https://doi.org/10.1523/JNEUROSCI.1592-12.2012 (2012).

18. Liu-Yesucevitz, L. et al. Tar DNA binding protein-43 (TDP-43) associates with stress granules: Analysis of cultured cells and pathological brain tissue. *PLoS One* **5**, e13250. https://doi.org/10.1371/journal.pone.0013250 (2010).
19. Vanderweyde, T. et al. Interaction of tau with the RNA-binding protein TIA1 regulates tau pathophysiology and toxicity. *Cell Rep.* **15**, 1455–1466. https://doi.org/10.1016/j.celrep.2016.04.045 (2016).
20. Iliyasu, M. O., Musa, S. A., Oladele, S. B. & Iliya, A. I. Amyloid-beta aggregation implicates multiple pathways in Alzheimer's disease: Understanding the mechanisms. *Front. Neurosci.* **17**, 1081938. https://doi.org/10.3389/fnins.2023.1081938 (2023).
21. Goswami, P. et al. Involvement of endoplasmic reticulum stress in amyloid beta ((1–42))-induced Alzheimer's like neuropathological process in rat brain. *Brain. Res. Bull.* **165**, 108–117. https://doi.org/10.1016/j.brainresbull.2020.09.022 (2020).
22. Cheignon, C. et al. Oxidative stress and the amyloid beta peptide in Alzheimer's disease. *Redox. Biol.* **14**, 450–464. https://doi.org/10.1016/j.redox.2017.10.014 (2018).
23. Mokas, S. et al. Uncoupling stress granule assembly and translation initiation inhibition. *Mol. Biol. Cell* **20**, 2673–2683. https://doi.org/10.1091/mbc.e08-10-1061 (2009).
24. Patel, J. et al. Cellular stresses profoundly inhibit protein synthesis and modulate the states of phosphorylation of multiple translation factors. *Eur. J. Biochem.* **269**, 3076–3085. https://doi.org/10.1046/j.1432-1033.2002.02992.x (2002).
25. Kumar-Singh, S. et al. In vitro studies of Flemish, Dutch, and wild-type beta-amyloid provide evidence for two-staged neurotoxicity. *Neurobiol. Dis.* **11**, 330–340. https://doi.org/10.1006/nbdi.2002.0529 (2002).
26. Shahnawaz, M., Thapa, A. & Park, I. S. Stable activity of a deubiquitylating enzyme (Usp2-cc) in the presence of high concentrations of urea and its application to purify aggregation-prone peptides. *Biochem. Biophys. Res. Commun.* **359**, 801–805. https://doi.org/10.1016/j.bbrc.2007.05.186 (2007).
27. Ukhueduan, B., Chukwurah, E. & Patel, R. C. Regulation of PKR activation and apoptosis during oxidative stress by TRBP phosphorylation. *Int. J. Biochem. Cell Biol.* **137**, 106030. https://doi.org/10.1016/j.biocel.2021.106030 (2021).
28. Shimazawa, M., Ito, Y., Inokuchi, Y. & Hara, H. Involvement of double-stranded RNA-dependent protein kinase in ER stress-induced retinal neuron damage. *Invest. Ophthalmol. Vis. Sci.* **48**, 3729–3736. https://doi.org/10.1167/iovs.06-1122 (2007).
29. Patel, C. V., Handy, I., Goldsmith, T. & Patel, R. C. PACT, a stress-modulated cellular activator of interferon-induced double-stranded RNA-activated protein kinase, PKR. *J. Biol. Chem.* **275**, 37993–37998. https://doi.org/10.1074/jbc.M004762200 (2000).
30. Sanchez, I. I. et al. Huntington's disease mice and human brain tissue exhibit increased G3BP1 granules and TDP43 mislocalization. *J. Clin. Invest.* https://doi.org/10.1172/JCI140723 (2021).
31. Gordiyenko, Y., Llacer, J. L. & Ramakrishnan, V. Structural basis for the inhibition of translation through eIF2alpha phosphorylation. *Nat. Commun.* **10**, 2640. https://doi.org/10.1038/s41467-019-10606-1 (2019).
32. Jiang, Z. et al. eIF2alpha Phosphorylation-dependent translation in CA1 pyramidal cells impairs hippocampal memory consolidation without affecting general translation. *J. Neurosci.* **30**, 2582–2594. https://doi.org/10.1523/JNEUROSCI.3971-09.2010 (2010).
33. Al Adem, K. & Lee, S. Structural polymorphism and cytotoxicity of brain-derived beta-amyloid extracts. *Protein Sci.* **32**, e4639. https://doi.org/10.1002/pro.4639 (2023).
34. Ono, K., Condron, M. M. & Teplow, D. B. Structure-neurotoxicity relationships of amyloid beta-protein oligomers. *Proc. Natl. Acad. Sci. U. S. A.* **106**, 14745–14750. https://doi.org/10.1073/pnas.0905127106 (2009).
35. Stefani, M. Structural features and cytotoxicity of amyloid oligomers: Implications in Alzheimer's disease and other diseases with amyloid deposits. *Prog. Neurobiol.* **99**, 226–245. https://doi.org/10.1016/j.pneurobio.2012.03.002 (2012).
36. Ghosh, S. & Geahlen, R. L. Stress granules modulate SYK to cause microglial cell dysfunction in Alzheimer's disease. *EBioMedicine* **2**, 1785–1798. https://doi.org/10.1016/j.ebiom.2015.09.053 (2015).
37. Lourenco, M. V. et al. TNF-alpha mediates PKR-dependent memory impairment and brain IRS-1 inhibition induced by Alzheimer's beta-amyloid oligomers in mice and monkeys. *Cell Metab.* **18**, 831–843. https://doi.org/10.1016/j.cmet.2013.11.002 (2013).
38. Wang, Z., Natte, R., Berliner, J. A., van Duinen, S. G. & Vinters, H. V. Toxicity of Dutch (E22Q) and Flemish (A21G) mutant amyloid beta proteins to human cerebral microvessel and aortic smooth muscle cells. *Stroke* **31**, 534–538. https://doi.org/10.1161/01.str.31.2.534 (2000).
39. Nunomura, A. et al. Involvement of oxidative stress in Alzheimer disease. *J. Neuropathol. Exp. Neurol.* **65**, 631–641. https://doi.org/10.1097/01.jnen.0000228136.58062.bf (2006).
40. Salminen, A., Kauppinen, A., Suuronen, T., Kaarniranta, K. & Ojala, J. ER stress in Alzheimer's disease: A novel neuronal trigger for inflammation and Alzheimer's pathology. *J. Neuroinflamm.* **6**, 41. https://doi.org/10.1186/1742-2094-6-41 (2009).
41. Mairet-Coello, G. & Polleux, F. Involvement of "stress-response" kinase pathways in Alzheimer's disease progression. *Curr. Opin Neurobiol.* **27**, 110–117. https://doi.org/10.1016/j.conb.2014.03.011 (2014).
42. Ferrer, I. Stress kinases involved in tau phosphorylation in Alzheimer's disease, tauopathies and APP transgenic mice. *Neurotox Res.* **6**, 469–475. https://doi.org/10.1007/BF03033283 (2004).
43. Bomfim, T. R. et al. An anti-diabetes agent protects the mouse brain from defective insulin signaling caused by Alzheimer's disease-associated Abeta oligomers. *J. Clin. Invest.* **122**, 1339–1353. https://doi.org/10.1172/JCI57256 (2012).
44. Talbot, K. et al. Demonstrated brain insulin resistance in Alzheimer's disease patients is associated with IGF-1 resistance, IRS-1 dysregulation, and cognitive decline. *J. Clin. Invest.* **122**, 1316–1338. https://doi.org/10.1172/JCI59903 (2012).
45. Tamagno, E. et al. Multiple signaling events in amyloid beta-induced, oxidative stress-dependent neuronal apoptosis. *Free Radic. Biol. Med.* **35**, 45–58. https://doi.org/10.1016/s0891-5849(03)00244-2 (2003).
46. Resende, R., Ferreiro, E., Pereira, C. & Oliveira, C. R. ER stress is involved in Abeta-induced GSK-3beta activation and tau phosphorylation. *J. Neurosci. Res.* **86**, 2091–2099. https://doi.org/10.1002/jnr.21648 (2008).
47. Suen, K. C., Yu, M. S., So, K. F., Chang, R. C. & Hugon, J. Upstream signaling pathways leading to the activation of double-stranded RNA-dependent serine/threonine protein kinase in beta-amyloid peptide neurotoxicity. *J. Biol. Chem.* **278**, 49819–49827. https://doi.org/10.1074/jbc.M306503200 (2003).
48. Peel, A. L. & Bredesen, D. E. Activation of the cell stress kinase PKR in Alzheimer's disease and human amyloid precursor protein transgenic mice. *Neurobiol. Dis.* **14**, 52–62. https://doi.org/10.1016/s0969-9961(03)00086-x (2003).
49. Paquet, C. et al. The PKR activator PACT is induced by Abeta: Involvement in Alzheimer's disease. *Brain Pathol.* **22**, 219–229. https://doi.org/10.1111/j.1750-3639.2011.00520.x (2012).
50. Chromy, B. A. et al. Self-assembly of Abeta(1–42) into globular neurotoxins. *Biochemistry* **42**, 12749–12760. https://doi.org/10.1021/bi030029q (2003).
51. Bellucci, A., Fiorentini, C., Zaltieri, M., Missale, C. & Spano, P. The, "in situ" proximity ligation assay to probe protein-protein interactions in intact tissues. *Methods Mol. Biol.* **1174**, 397–405. https://doi.org/10.1007/978-1-4939-0944-5_27 (2014).
52. Ciani, C., Pistorio, G., Mearelli, M. & Falcone, C. Immunofluorescence protocol for localizing protein targets in brain tissue from diverse model and non-model mammals. *STAR Protoc.* **4**, 102482. https://doi.org/10.1016/j.xpro.2023.102482 (2023).

Acknowledgements

This work is supported by the National Research Foundation of Korea (NRF), funded by the Ministry of Education (NRF-2022R1I1A1A01068270) and Ministry of Science and ICT (RS-2023-00209274 and RS-2022-NR070848). We thank Prof. Park Il Seon for the Aβ42 constructs.

Author contributions

V.R. and T.O. conceived the project. V.R. carried out the experiments, data acquisition, figure, and manuscript preparation. A.B. helped with animal experiment. M.C. provided valuable discussions. T.O. supervised, revised, and approved the final version of the manuscript. All authors read and approved the final manuscript.

Declarations

Competing interests

The authors declare no competing interests.

Additional information

Supplementary Information The online version contains supplementary material available at https://doi.org/10.1038/s41598-025-88380-y.

Correspondence and requests for materials should be addressed to V.S.R. or T.O.

Reprints and permissions information is available at www.nature.com/reprints.

Publisher's note Springer Nature remains neutral with regard to jurisdictional claims in published maps and institutional affiliations.